

Christoph Eyberg*, Ashkan Shiravand,
Patrick Klemm, Johannes Horsch, Giorgio
Cattaneo and Jens Langejürgen

A Feasibility Study of Fluoroscopy-based Catheter Modeling

<https://doi.org/10.1515/cdbme-2024-1004>

Abstract: Knowledge of contact forces between instruments and blood vessels during endovascular interventions like thrombectomies can help make these interventions safer and faster. We show that it is generally feasible to derive the contact forces directly from the intraoperative fluoroscopy imaging system which can make the costly integration of additional sensors into catheters and guidewires dispensable. Our study is limited to stationary normal loading and planar deflections. In our loading scenario of crossing the carotid siphon with a guidewire, the magnitude of contact forces can be detected up to an average deviation of 4.5 % for an image-based pose measurement accuracy of the guidewire of 1 mm.

Keywords: endovascular, force from shape, flexible instruments, force sensing.

1 Introduction

Minimal-invasive surgery methods are known for lower trauma and, therefore, faster patient rehabilitation. For vascular diseases like ischemic heart or strokes, which are the leading causes of death worldwide, endovascular interventions have become the gold standard for many diagnostic or therapeutic interventions.

During endovascular interventions, guidewires and catheters, which are very long and slender instruments, are navigated from an insertion point at the groin or arm through the vascular system to the point where, e.g., the thrombus is removed. The interventions are usually performed under

fluoroscopy imaging, which allows the physicians to observe the current position and orientation of the instruments inside the body in real-time.

As the instruments are bent throughout the tortuous vascular systems, the control of the instrument from the proximal end outside the body becomes increasingly indirect. Also, the haptic feedback experienced at the proximal end of the instrument is limited as it represents the accumulated contact forces along the instrument's whole shaft. As time is of crucial importance in these interventions, additional information on the instrument's behavior and interaction with the surrounding tissue can help choose suitable navigation maneuvers to reach the target area faster and prevent vessel damage by warning in case of dangerous situations like high force being exerted onto the vascular walls. To provide such information, measuring the contact forces between the catheter and the vessel walls is necessary.

So far, most research has focused on including miniature sensors in catheters and guidewires. There are commercially available ablation catheters that measure the contact force at the tip during ablation to control the outcome [1], and multiple researchers have shown the possibility of including Fiber-Bragg-Grating (FBG) sensors along the whole endovascular instrument and their capability for force measurement [2]. A problem with this approach is that it makes these single-use instruments very expensive.

Some researchers have shown the feasibility of deriving the applied contact forces from the measured shape of continuum robots [3]. Flexible endovascular Instruments can be modelled analogously but are usually prone to larger deformations than those analyzed in these studies. We, therefore, evaluated the general feasibility and potential accuracy of deriving the contact forces between a guidewire and the vessel walls using only the existing fluoroscopy imaging system in a realistic setup. Hence, we created a realistic intraoperative guidewire deflection using a vessel phantom made from hydrogel and retrieved the contact forces manually using a mechanical model. We then measure the sensitivity of the guidewire deflection within the model to force changes. This allowed us to obtain the possible accuracy of force measurements from the given image resolution of angiography systems.

The remainder of this paper is structured as follows: In 2.1, we give a short introduction to the mechanical model that is used for modelling the guidewire. Afterwards, in 2.2, we describe the fabrication of the hydrogel vessel phantoms and present the experimental setup in 2.3. The results of the experiments are given in 3 and discussed in 4.

*Corresponding author: **Christoph Eyberg:** Fraunhofer IPA, Theodor-Kutzer-Ufer 1-3, Mannheim, Germany, e-mail: Christoph.Eyberg@ipa.fraunhofer.de

Ashkan Shiravand, Giorgio Cattaneo: Institute of Biomedical Engineering, University of Stuttgart, Stuttgart, Germany

Patrick Klemm, Johannes Horsch, Jens Langejürgen: Fraunhofer IPA, Mannheim, Germany

2 Methods

2.1 Cosserat Rod Theory

Endovascular instruments are long and slender devices which are prone to large deformations. We, therefore, used the nonlinear Cosserat Rod theory in static form, as presented in [4], to model the guidewire in our experiments. The points along the rod's centerline can be parameterized as $\mathbf{r}(s)$ with s being the arc-length parameter. Likewise, the orientation of each fragment along the rod can be described using a rotation matrix $R(s)$ with respect to a chosen coordinate system. The z-axis of each local coordinate system is hereby fixed to the orientation of the rod. The local curvature vector is defined by

$$\mathbf{u}(s) = \left(R^T(s) \dot{R}(s) \right)^\sim \quad (1)$$

with the (\sim) operator converting an element of $SO(3)$ to \mathbf{R}^3 (while $(\widehat{\cdot})$ is the inverse operator) and the $(\dot{\cdot})$ specifying a derivation along the arc-length of the rod.

As we neglect axial elongation and transverse shear strain, the pose and orientation of the rod can be calculated based on the differential equations

$$\dot{\mathbf{r}}(s) = R(s) \mathbf{e}_3 \quad (2)$$

$$\dot{R}(s) = R(s) \hat{\mathbf{u}}(s). \quad (3)$$

To solve this, the curvature $\mathbf{u}(s)$ can be calculated from the constitutive law that assumes fully elastic deformation with the stiffness matrix \mathbf{K} . The moments in global coordinates are

$$\mathbf{m}(s) = R(s) \mathbf{K}(s) \Delta \mathbf{u}(s) \quad (4)$$

where $\Delta \mathbf{u}(s) = \mathbf{u}(s) - \mathbf{u}^\circ(s)$ with \mathbf{u}° denoting the resting curvature. Taking the derivative with respect to s gives

$$\dot{\mathbf{m}} = R \left((\mathbf{K}(\dot{\mathbf{u}} - \dot{\mathbf{u}}^\circ) + (\hat{\mathbf{u}}\mathbf{K} + \dot{\mathbf{K}})(\mathbf{u} - \mathbf{u}^\circ) \right). \quad (5)$$

To obtain this inner moment \mathbf{m} from external forces \mathbf{f} we cut the rod at an arbitrary point s and formulate the balances of forces (6) and moments (7)

$$\int_s^l \mathbf{f}(\sigma) d\sigma - \mathbf{n}(s) = 0 \quad (6)$$

$$\int_s^l \mathbf{r}(\sigma) \times \mathbf{f}(\sigma) d\sigma - \mathbf{m}(s) - \mathbf{r}(s) \times \mathbf{n}(s) = 0. \quad (7)$$

Taking the derivative of both and combining the results gives

$$\dot{\mathbf{m}}(s) + \dot{\mathbf{r}}(s) \times \int_s^l \mathbf{f}(\sigma) d\sigma = 0. \quad (8)$$

This relationship can be combined with the moment balance from the constitutive law to obtain a differential equation for the local curvature

$$\begin{aligned} \dot{\mathbf{u}} = \dot{\mathbf{u}}^\circ - \mathbf{K}^{-1} \left((\hat{\mathbf{u}}\mathbf{K} + \dot{\mathbf{K}})(\mathbf{u} - \mathbf{u}^\circ) \right. \\ \left. + \hat{\mathbf{e}}_3 R^T \int_s^l \mathbf{f}(\sigma) d\sigma \right). \end{aligned} \quad (9)$$

Together (2), (3), and (9) form a closed set of differential equations that can be solved as an initial value problem. [4]

2.2 Hydrogel Vascular Model

To retrieve a realistic deflection of guidewires, we modelled a standardized form of the carotid siphon on a single plane [5]. This is a crucial vessel section for navigation during endovascular stroke treatment. The vessel phantoms were created using combined 3d printing, casting and molding technologies in the forms of cuboid and thin-wall vessels. While the block phantoms represented the behavior of blood vessels that had limited flexibility, like those that were surrounded by bones, the thin wall phantoms allowed for higher flexibility as if the vessels were surrounded by soft tissue. The vessel lumen geometry was designed with diameters of 3.5 and 5.5 mm. The designed vessel lumens were printed out of "Grey" resin using a stereolithography 3d printer (Form 3, Formlabs Inc., MA, USA). Tissue-mimicking material, representing block and thin-wall phantoms, respectively, was composed of polyvinyl alcohol hydrogel (PVA-H) with 10 and 17 wt% PVA powder (Mw 85k-124k g/mol, Merck KGaA, Germany), and dissolved in a 20/80 wt% water/dimethyl sulfoxide solution (Merck KGaA, Germany) at the temperature of 120°C until the complete dissolution of the PVA. The prepared gel was placed in a vacuum chamber to remove any enclosed air bubbles and then filled into a mold, placing the 3D-printed vessel core in the center of the mold. All molds were then subjected to five freeze-thaw cycles, freezing at -22°C for 18 hours and following thawing at room temperature for 6 hours. Afterwards, the vessel core was removed, leaving a vessel closely resembling human blood vessels' physiological compliance [6].

2.3 Experimental Setup

Guidewires are usually designed to have areas of different stiffness, being especially soft at the J-shaped tip. For simplicity, we neglected the tip and used a nitinol wire of 0.2mm (or 0.6Fr) constant diameter for our experiments. Young's modulus of the whole wire was determined to be 84.3 GPa in a bending test. We applied a 3D-printed soft tip to the 136 mm long wire to avoid damaging the sensitive hydrogel phantoms and guided it through the vessels as shown in Figure 1. In this static setup, we placed the phantom and wire into a water bath for better visibility and then performed fluoroscopy-imaging using an Artis-zeego angiography



Figure 1: Experimental setup before insertion into water bath.

system (Siemens Healthineers). We afterwards used the image processing tools from [7] to detect the guidewire, retrieve the centerline coordinates from the image, and transform them into lab coordinates.

To reconstruct the unknown loading in our mechanical model, we made the following assumptions: We neglected friction forces, as guidewires are usually designed with a hydrophilic coating that provides a lubrication film around the guidewire to assert low friction at the contacts. We also assumed that each force F_i was concentrated at a single point s_i . While this is a simplification of the true contacts where the contact area increases due to the flexibility of the vessels, it provides a conservative force estimation among the non-unique set of solutions for this inverse problem and is capable of closely resembling the measured wire deflection.

We then manually tuned the position and magnitude of forces along the modelled guidewire until it resembled the same shape as the guidewire in the phantom and took this loading with F_i^* with $i \in [1,6]$ as the ground truth pose r^* . To assess the sensitivity of a fluoroscopy-based force measurement approach we identified possible sources of error. Such sources of error might be:

- Limited resolution of the imaging system
- Limited knowledge of the mechanical properties of the endovascular instruments
- Out-of-plane deflection of the instruments

The error of out-of-plane deflection did not apply to our planar model and was, therefore, not considered. Minimizing it in other scenarios is possible, e.g., by adjusting the measurement plane or using modern biplane angiography systems. Also, knowledge of the instrument's mechanical properties is a prerequisite for measurement approaches using sensors like FBGs. Therefore, we focused on the first source of error – the imaging system's resolution. Depending on the exact position of the vessels between the tube and detector of the C-arm of an Artis Zeego, the fluoroscopy can cover an area of up to about 250x250 mm². With an image resolution of 512x512 px² this gives a resolution of 2 px/mm. We, therefore, assumed a pose measurement accuracy of the guidewire of $\Delta r_{\text{fluoro}} = 0.5$ mm and also evaluated a pessimistic scenario with an accuracy of $\Delta r_{\text{fluoro}} = 1$ mm e.g. to account for additional unknown errors in the measurement process.

Using the mechanical model, we individually varied the previously reconstructed forces and their application points, keeping the remaining forces fixed until the distance between the new guidewire pose and the ground truth pose exceeded the measurable pose change (10), as shown in Figure 2.

$$\max_s \|\mathbf{r}^*(s, \mathbf{F}^*) - \mathbf{r}(s, \mathbf{F}^* + \Delta \mathbf{F})\| \geq \Delta r_{\text{fluoro}} \quad (10)$$

As the deflection accumulates with increasing distance and can be partially compensated by changes in the magnitude of the remaining forces, we measured the error only in the area

between the guidewire tip and the application point of the second force following the altered force (in the direction from the tip to base). Additionally, we repeated the assessment by varying two consecutive forces inversely ($\Delta \mathbf{F}_{i+1}^{\text{combined}} = -\Delta \mathbf{F}_i^{\text{combined}}$) to account for the possible compensation of errors.

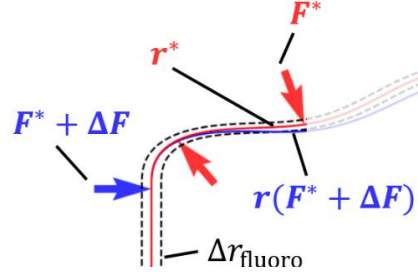


Figure 2: Each force is varied until the offset between the new pose (blue) and the ground truth pose (red) would be detectable on the fluoroscopy image in the local area

3 Results

The measured shape from inside the hydrogel phantoms is reproduced by the model with manually tuned forces with an average deviation below the measurement accuracy. The exact values of the deviation are given in Table 1.

Table 1: Difference between centerline points extracted from fluoroscopy image and centerline points of mechanical model with reconstructed forces F_i^* in four loading scenarios j

j	Vessel Model	Average Error	Maximum Error
1	Block 3.5	0.3 mm	0.6 mm
2	Block 5.5	0.2 mm	0.4 mm
3	Wall 3.5	0.2 mm	0.3 mm
4	Wall 5.5	0.2 mm	0.3 mm

The forces' number, position and direction are coherent with the observable contacts in the fluoroscopy image. The forces range between 0.03 N and 0.18 N, with larger forces for the block models and the small vessel diameter than for the wall models and the larger diameter because the wall model deforms stronger under the contacts, and the larger vessel diameter induces less deflection of the guidewire.

When varying the forces in the loading scenarios of the four hydrogel phantoms j , the change in position of the guidewire reaches a detectable offset at a force-error of on average 3 mN or 4.5 % of the force magnitude for $\Delta r_{\text{fluoro}} = 1$ mm and of 1.5 mN (2.2 %) with $\Delta r_{\text{fluoro}} = 0.5$ mm. The sensitivity towards these errors varies significantly among the different forces, as shown by the minimum and maximum detectable errors in Table 2 and the results for scenario $j = 1$ in Table 3.

Table 2: Smallest detectable measurement errors, Min, max and mean values among all forces in the four loading scenarios.

Δr_{fluoro}		ΔF_{min}		Δs_{min}		$\Delta F_{\text{min}}^{\text{combined}}$	
		[mN]	[%]	[mm]	[%]	[mN]	[%]
1 mm	min _{i,j}	0.32	0.42	0.04	0.03	0.68	1.26
	max _{i,j}	10.36	14.47	2.03	1.49	7.67	15.54
	mean _{i,j}	3.06	4.46	0.43	0.32	3.44	4.66
0.5 mm	min _{i,j}	0.02	0.18	0.04	0.03	0.34	0.63
	max _{i,j}	5.30	7.19	0.98	0.72	3.95	7.72
	mean _{i,j}	1.54	2.24	0.25	0.19	1.70	2.31

This is due to the geometrical nonlinearity induced by the large deflection and to the differences in magnitude of the forces e.g. the largest relative force error (14.5 %) corresponds to one of the smallest forces ($\|F_i^*\| = 4$ mN). The deflection reacts very sensitively towards the variation of the application points as, on average, a change of 0.4 mm or 0.3 % of the wire length (0.3 mm, 0.2% for $\Delta r_{\text{fluoro}} = 0.5$ mm) is detectable. This change in application point not only alters the lever for the bending moment but can also shift the direction of the applied force, which is assumed to be normal to the guidewire.

Table 3: Force magnitudes and their application point as arc-length distance from tip for the 3.5 mm wall phantom and their smallest detectable measurement error for 1 mm pose accuracy.

i	F_i	s_i	$\Delta F_{i,\text{min}}$		$\Delta s_{i,\text{min}}$		$\Delta F_{i,\text{min}}^{\text{combined}}$	
			[mN]	[%]	[mm]	[%]	[mN]	[%]
1	38.10	32.24	2.42	6.36	0.56	0.42	2.88	7.57
2	-101.13	44.88	2.25	2.23	0.32	0.24	2.88	2.85
3	97.76	55.70	1.57	1.61	0.24	0.18	2.87	2.93
4	-56.49	70.45	2.57	4.54	0.04	0.003	1.81	3.21
5	53.69	84.42	0.32	0.59	0.24	0.18	0.68	1.27
6	-30.45	94.46	0.59	1.96	0.42	0.31	0.68	0.22

While the average error for the combined force variation increases slightly due to compensation, the spread between min and max decreases as the more sensitive of the two neighboring forces dominates. Within the range of errors and individually for each force, the relationship between accuracy in image processing and detectable error is almost linear.

4 Conclusion

We have shown that retrieving the contact forces between endovascular instruments and blood vessels directly from

fluoroscopy images is generally possible. With the worst deviation from the real force magnitude of 15.5 %, this matches the precision of the force measurement using integrated FBGs [2], and with an average error of 3 mN, this approach has the potential to yield the same accuracy as the commercially available catheter with tip sensing [1] without the need for expensive additional sensors. Yet, these results are limited by the assumptions of planar deflections, stationary loading, and the neglect of axial forces like tip forces or friction, which could only be detected if they occur on pre-bend wires. In a real-world application, other types of error, e.g. in the assumed mechanical properties or insufficient convergence of the force detection algorithm, might additionally occur. Our future work will, therefore, focus on the remaining challenges in fluoroscopy-based force detection: forces that cause out-of-image-plane bending and dynamical modelling of the loading scenario.

Author Statement

Research funding: This project is funded by the Leistungszentrum Mass Personalization

Conflict of interest: Authors state no conflict of interest.

References

- [1] Kueffer T, Haeberlin A, Knecht S et al. (2023) Validation of the accuracy of contact force measurement by contemporary force-sensing ablation catheters. *J Cardiovasc Electrophysiol* 34:292–299. <https://doi.org/10.1111/jce.15770>
- [2] Qiao Q, Borghesan G, Schutter J de et al. (2021) Force from Shape—Estimating the Location and Magnitude of the External Force on Flexible Instruments. *IEEE Trans Robot* 37:1826–1833. <https://doi.org/10.1109/TRO.2021.3062504>
- [3] Aloï V, Dang KT, Barth EJ et al. (2022) Estimating Forces Along Continuum Robots. *IEEE Robot Autom Lett* 7:8877–8884. <https://doi.org/10.1109/LRA.2022.3188905>
- [4] Rucker DC, Jones BA, Webster RJ (2010) A Geometrically Exact Model for Externally Loaded Concentric-Tube Continuum Robots. *IEEE Trans Robot* 26:769–780. <https://doi.org/10.1109/TRO.2010.2062570>
- [5] Vijaywargiya M, Deopujari R, Athavale SA (2017) Anatomical study of petrous and cavernous parts of internal carotid artery. *Anat Cell Biol* 50:163–170. <https://doi.org/10.5115/acb.2017.50.3.163>
- [6] Kosukegawa H, Shida S, Hashida Y et al. Mechanical Properties of Tube-Shaped Poly (Vinyl Alcohol) Hydrogel Blood Vessel Biomodel. In: *American Society of Mechanical Engineers 2010 – ASME 2010 3rd Joint US-European Fluids Engineering Summer Meeting*, pp 1877–1883. <https://doi.org/10.1115/FEDSM-ICNMM2010-30892>
- [7] Eyberg C, Karstensen L, Pusch T et al. (2022) A ROS2-based Testbed Environment for Endovascular Robotic Systems. *Current Directions in Biomedical Engineering* 8:89–92. <https://doi.org/10.1515/cdbme-2022-0023>